iScience

CellPress
OPEN ACCESS

Article

Transcriptomic profiling reveals sex-specific molecular signatures of adipose endothelial cells under obesogenic conditions

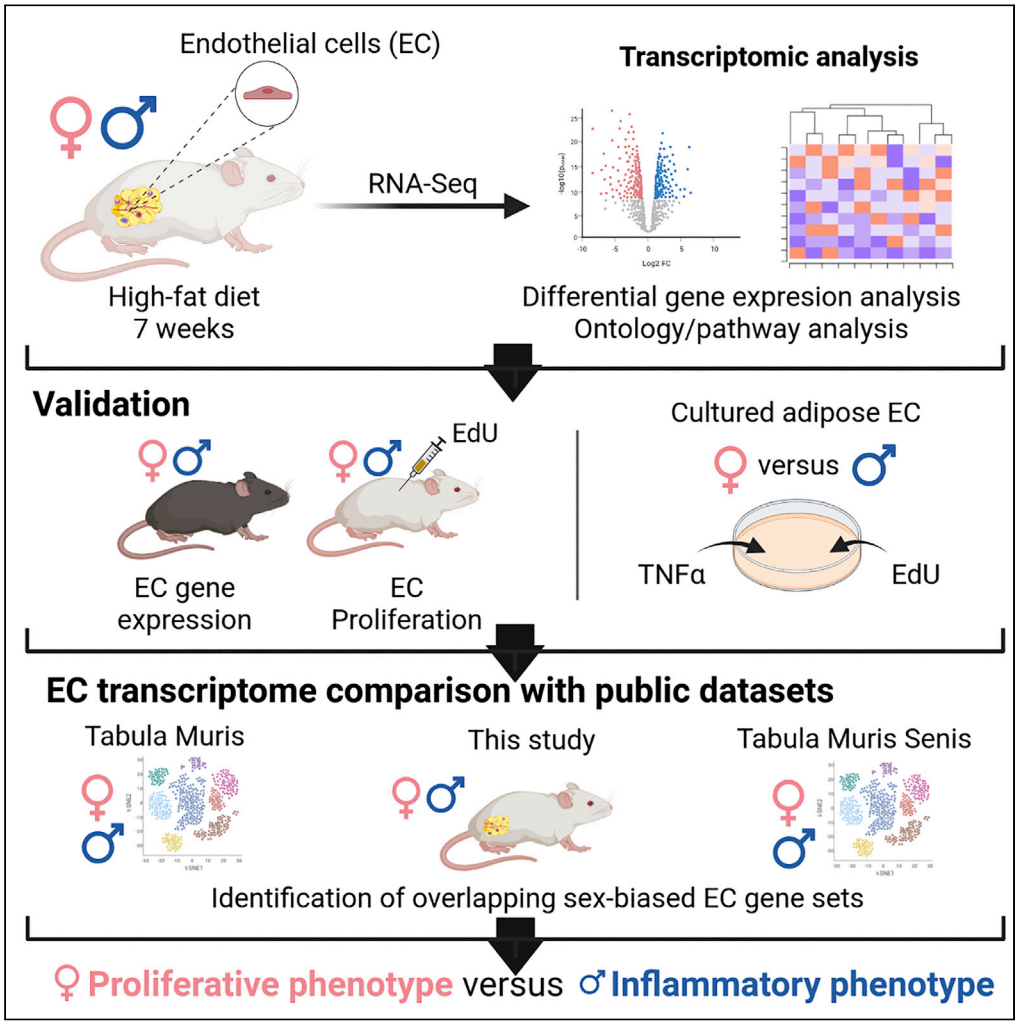

Martina Rudnicki, Alexandra Pislaru, Omid Rezvan, ..., Emilie Roudier, Thomas Gustafsson, Tara L. Haas

m.rudnicki@ucl.ac.uk (M.R.)
thaas@yorku.ca (T.L.H.)

Highlights

Adipose-derived endothelial cells from obese mice possess sex-biased transcriptomes

Female endothelial cells from white adipose tissue are more proliferative than male

An inflammatory phenotype is prominent in male adipose-derived endothelial cells

Sex-biased characteristics are retained in cultured adipose endothelial cells

Rudnicki et al., iScience 26, 105811
January 20, 2023
https://doi.org/10.1016/j.isci.2022.105811

iScience

CellPress
OPEN ACCESS

Article

Transcriptomic profiling reveals sex-specific molecular signatures of adipose endothelial cells under obesogenic conditions

Martina Rudnicki,[1,4,5,*] Alexandra Pislaru,[2,5] Omid Rezvan,[1] Eric Rullman,[3] Aly Fawzy,[1] Emmanuel Nwadozi,[1] Emilie Roudier,[1] Thomas Gustafsson,[3] and Tara L. Haas[1,2,6,*]

SUMMARY

Female mice display greater adipose angiogenesis and maintain healthier adipose tissue than do males upon high-fat diet feeding. Through transcriptome analysis of endothelial cells (EC) from the white adipose tissue of male and female mice high-fat-fed for 7 weeks, we found that adipose EC exhibited pronouncedly sex-distinct transcriptomes. Genes upregulated in female adipose EC were associated with proliferation, oxidative phosphorylation, and chromatin remodeling contrasting the dominant enrichment for genes related to inflammation and a senescence-associated secretory of male EC. Similar sex-biased phenotypes of adipose EC were detectable in a dataset of aged EC. The highly proliferative phenotype of female EC was observed also in culture conditions. In turn, male EC displayed greater inflammatory potential than female EC in culture, based on basal and tumor necrosis factor alpha-stimulated patterns of gene expression. Our study provides insights into molecular programs that distinguish male and female EC responses to pathophysiological conditions.

INTRODUCTION

Endothelial cells (EC) form the contiguous inner lining of the entire circulatory system. Within this privileged position as the interface between the bloodstream and all parenchymal cells, EC act as gatekeepers of energy balance and tissue homeostasis by controlling nutrient and oxygen supply, coagulation and inflammation.[1,2] EC provide additional support for tissue growth and metabolism by coordinating the growth of new capillaries through angiogenesis.[3] During this process, they exit their usual state of quiescence and adopt specialized transient phenotypes associated with proliferation and motility.[3,4] Moreover, EC exhibit organ-specific molecular signatures and functional specializations based on bidirectional paracrine interactions with the tissue parenchyma and adjacent stromal cells.

Extensive evidence from animal and human studies concur that EC dysfunction and impaired angiogenesis contribute to the development of obesity and its related complications.[5–8] In white adipose tissue of males, insufficient capillary growth compromises healthy tissue expansion to accommodate calorie excess, which ultimately reflects in metabolic disturbances at the systemic level. Our group and others have reported that promoting angiogenesis to increase adipose vascularization can prevent/reverse metabolic disorders associated with excess adiposity.[9–11] Although this reinforces the paramount role of adipose EC in the pathogenesis of obesity-related disease, the molecular profiles of adipose EC under conditions of obesity, and the extent to which biological variables may regulate their vulnerability to dysfunction have not been investigated.

Sex is a biological variable that accounts for differences in adipose tissue pathophysiology and clinical manifestations of obesity.[12] However, mechanisms underlying these differences are poorly defined particularly because sex is frequently overlooked in pre-clinical studies.[13,14] We recently provided the first evidence that female mice have greater adipose angiogenesis than males in response to high-fat diet (HFD) feeding, indicating that sex is a modifier of vascular remodeling. Yet, the underlying mechanisms for this difference remain unknown. Given that several recent studies have reported intrinsic sex differences in gene expression and behavior of human umbilical vein endothelial cells (HUVEC),[15–19] we hypothesize

[1]School of Kinesiology and Health Science & Muscle Health Research Centre, York University, Toronto, Canada

[2]Department of Biology, York University, Toronto, Canada

[3]Department Laboratory Medicine, Clinical Physiology, Karolinska Institutet and Department Clinical Physiology, Karolinska University Hospital, Stockholm, Sweden

[4]Present address: UCL Institute of Ophthalmology, University College London, London, UK

[5]These authors contributed equally

[6]Lead contact

*Correspondence: m.rudnicki@ucl.ac.uk (M.R.), thaas@yorku.ca (T.L.H.)

https://doi.org/10.1016/j.isci.2022.105811

that EC sex differences play a substantial role in establishing divergent angiogenic responses in the expanding adipose tissue.

Thus, the present study aimed to analyze the transcriptome of adipose tissue EC of male and female mice to identify molecular signatures that may determine the sex differences in vascular remodeling during HFD-induced expansion of white adipose tissue.

RESULTS

Male and female adipose endothelial cells exhibit distinct molecular profiles under obesogenic conditions

We recently reported that the expansion of the visceral adipose tissue of female mice is accompanied by a concomitant growth of its vascular network that contrasts with the compromised adipose angiogenesis of male mice following 16 weeks of HFD feeding.[20] Here, we sought to uncover predictive molecular mechanisms that may explain the disparate angiogenic capacity in adipose of female compared to male mice, by focusing on EC gene expression during an earlier phase of adipose tissue remodeling. Thus, we conditioned male and female FVB; B6 mice with a 7-week HFD intervention. Mouse body weight gain and plasma glucose levels of these mice are provided in Table S1. The transcriptome of EC isolated from white adipose tissue of these mice was analyzed by RNA-Sequencing (RNA-Seq). First, we examined the pattern of EC hallmark genes (Figure S1). As expected, transcripts for EC marker genes *Cdh5*, *Pecam1*, and *Ptprb* were abundant in both male and female EC. Capillary marker genes also were prominent whereas transcripts of arterial and venous EC markers were present at lower levels.

Differential gene expression analysis displayed substantial sex-dependent transcriptional differences in adipose EC, with 1,281 differentially expressed genes (DEGs) between the sexes when applying an adjusted p value of 0.01 as a cut-off (Figure 1A). The majority of the DEGs (1,225 genes) were distributed among autosomal chromosomes while 56 DEGs were detected on the X chromosome (Figure 1B). Genes localized to the Y chromosome were not included in the analysis.

Gene Ontology (GO) enrichment analysis of the RNA-Seq dataset was used to identify biological processes (BP) over-represented within the sets of DEGs for each sex. Genes associated with chromatin organization, epigenetic modifications, and transcriptional regulation were significantly enriched in the female EC DEGs (Figure 1C), and suggestive of elevated cellular proliferative activity. Female EC also exhibited an enrichment of the GO BP term "ossification," which largely included genes that have known EC expression and can influence mesenchymal cell behavior (i.e. *Ptn* and *Bmp3)*. Conversely, the DEGs that were higher in male EC were dominantly associated with GO BP terms related to inflammation. Interestingly, male EC were enriched in genes belonging to the contrasting ontologies of "negative" and "positive regulation of angiogenesis," which may imply a restriction on angiogenic signaling in these cells. Differing sets of genes encoding extracellular matrix (ECM) and adhesion proteins were enriched in female and male EC, respectively. Complete lists of the significantly enriched GO BPs for each sex are provided in Table S2. In sum, these data demonstrate that male and female EC display substantially distinct transcriptional profiles under high-fat feeding.

To verify that sex differences in gene expression detected in the RNA-Seq dataset were not limited only to this mouse cohort or strain, we conducted the qPCR analysis of selected genes utilizing adipose EC isolated from an independent cohort of 7-week HFD-fed male and female C57Bl6/J. Mouse body weight gain, fasting glucose, and glucose tolerance tests of this mouse cohort were reported in Table S3. Overall, a high level of consistency was observed between gene expression in this independent cohort compared with the RNA-Seq dataset, with 12 of the 14 genes tested displaying the same patterns of gene expression (Table S4).

Female adipose endothelial cells show a highly proliferative phenotype compared to male counterparts

Angiogenesis requires the transient acquisition of the specialized phenotypes of proliferating stalk and migratory tip cells,[3,4] which is supported by metabolic reprogramming.[3,21] Thus, we assessed within our RNA-Seq dataset the molecular profiles involved in supporting distinct cellular phenotypes and metabolic pathways. First, we conducted GSEA using gene sets comprising markers for proliferative and tip endothelial phenotypes (Table S5), hypothesizing that both would be enriched in female EC. Indeed, female EC

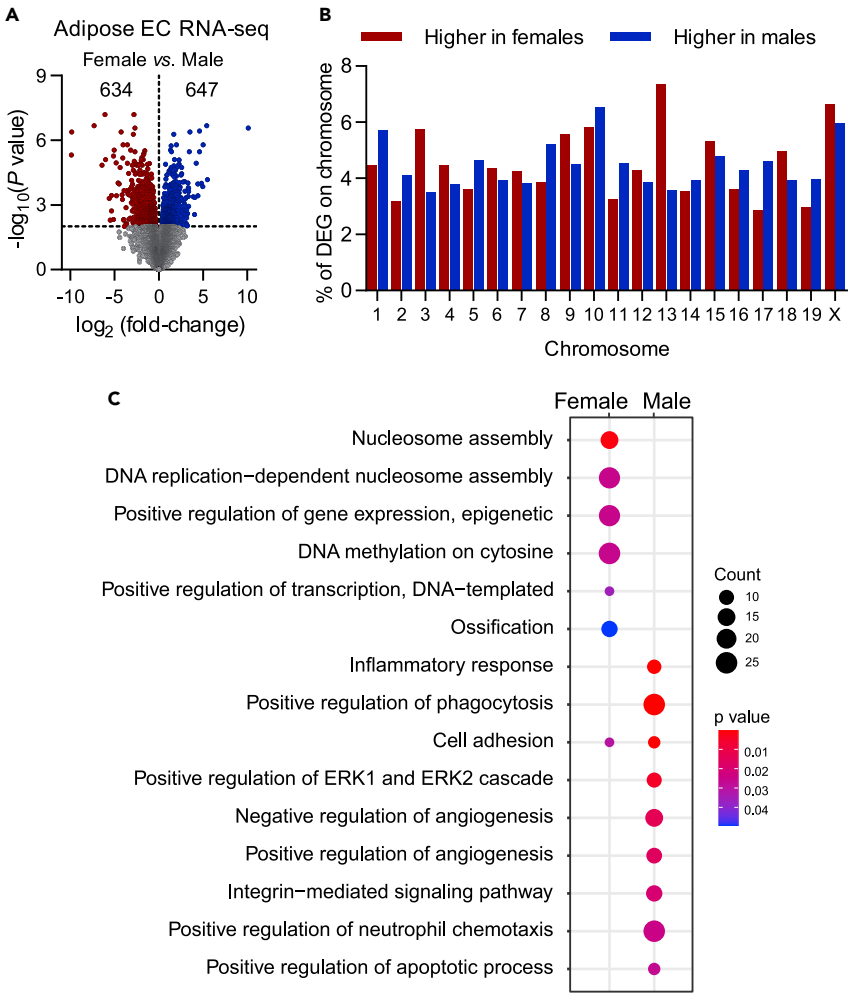

Figure 1. Transcriptome analysis of male and female adipose EC from HF-fed mice

(A) Volcano plot illustrating the expression profile of genes in female and male adipose EC, as determined by RNA-seq of n = 4 mice per sex. Negative logFC (red) = up in females; positive logFC (blue) = up in males. A total of 1,281 DEGs were identified, with an adjusted p value < 0.01 (indicated by the dashed horizontal line). See also Figure S1.

(B) Chromosome distribution of DEGs in female and male adipose EC. The proportions of female and male-biased genes are expressed as a % of the total number of genes on that chromosome.

(C) Dot plot illustrating selected "Biological Process" gene ontologies that were enriched in the DEG upregulated in female and male adipose EC, respectively. The count represents the number of inputted DEGs as a percentage of the total number of genes in that ontology. The Benjamini p value for each ontology is shown. All significant ontologies are listed in Table S3.

displayed enriched expression of genes associated with proliferation (Figures 2A and 2B). However, enrichment on tip cell genes was detected in male EC (Figures 2A and 2B). Despite the phenotype differences, the transcript levels of genes involved in glycolysis, pentose phosphate pathway, tricarboxylic acid cycle, or glutamine metabolism did not differ between male and female EC (Figure S2A). *In vitro* analysis of cultured male and female EC also did not display sex differences in protein levels of glycolytic markers hexokinase 2 (HK2), 6-phosphofructo-2-kinase/fructose-2,6-bisphosphatase 3 (PFKFB3), and Glyceraldehyde-3-Phosphate Dehydrogenase (GAPDH) (Figures S2B–S2D). In contrast, we observed a substantial enrichment of genes associated with oxidative phosphorylation in female EC (Figures 2A and 2B). This is notable because mitochondrial respiration was reported to be critical to sustain EC proliferation.[22]

To substantiate the greater proliferative potential of female EC under HFD conditions, we used a third cohort of mice that underwent a similar protocol of HF feeding for 7 weeks. Employing the nucleotide

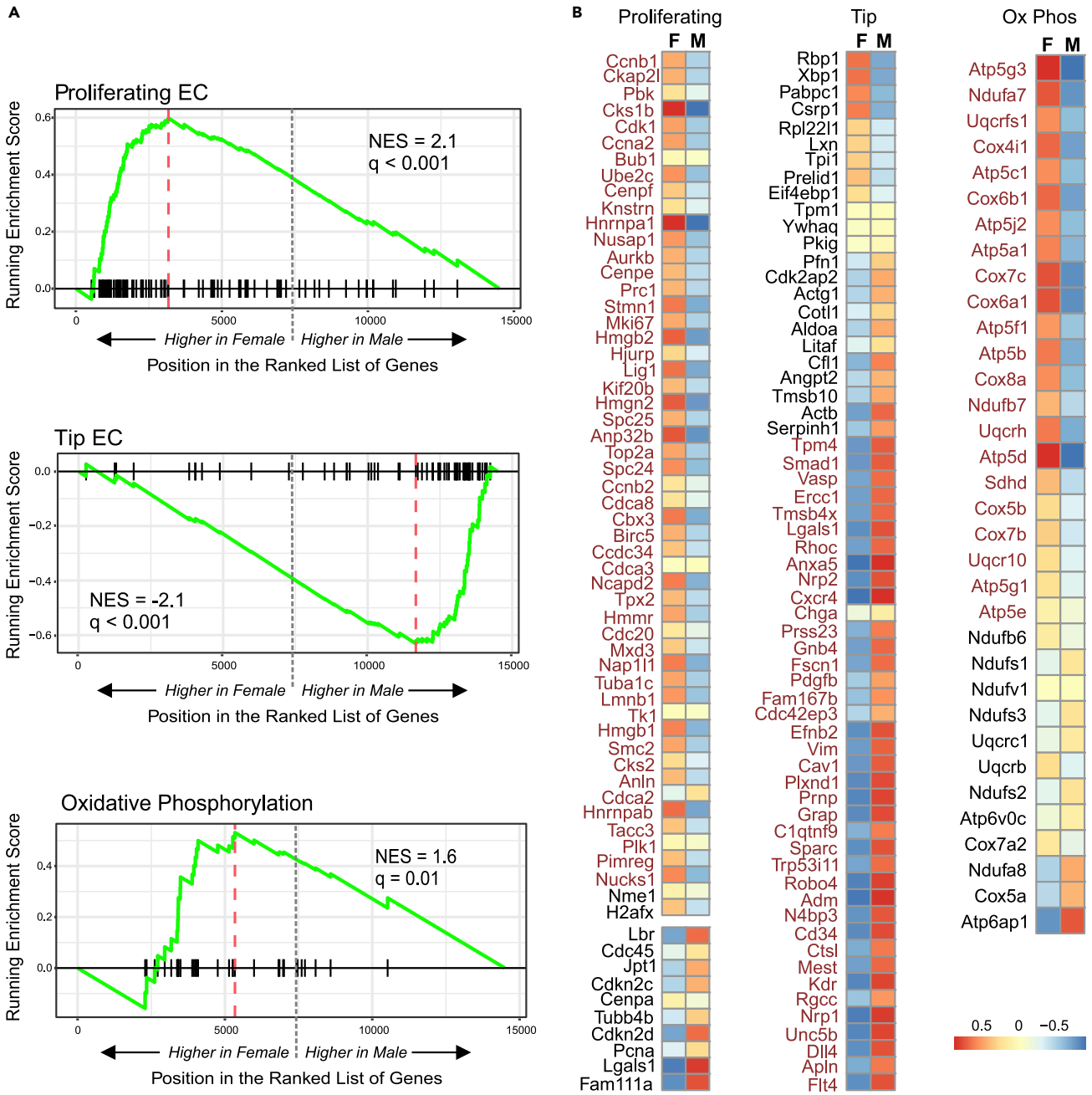

Figure 2. Female adipose EC exhibit elevated markers of proliferation and oxidative phosphorylation compared to male EC

(A and B) GSEA of endothelial cell proliferating, tip, and oxidative phosphorylation genes with corresponding heatmaps.

(A) GSEA plots of genes representing proliferating EC, mouse tip cell markers; and oxidative phosphorylation machinery.

(B) Heatmaps corresponding to the genes found in the GSEA plots in (A), displaying average z-scores for each sex, calculated from the gene TPM for each sample. Leading edge genes are indicated in red font. Full list in Table S5. See also Figure S2.

analogue EdU to mark cells in S-phase during the last week of the dietary intervention, coupled with ERG staining to identify EC nuclei, we detected proliferating EC in the visceral adipose of both sexes (Figure 3A). However, a significantly higher proportion of EC was EdU-positive in the white adipose of female mice, corroborating the gene expression analyses (Figure 3B). Of note, we did not detect differences in mRNA levels of key angiogenic factors *Vegfa* or *Vegfb*[10,11] between male and female white adipose tissue either in the cohort of mice used for the assessment of EdU incorporation (Figures 3C and 3D) or in those used for

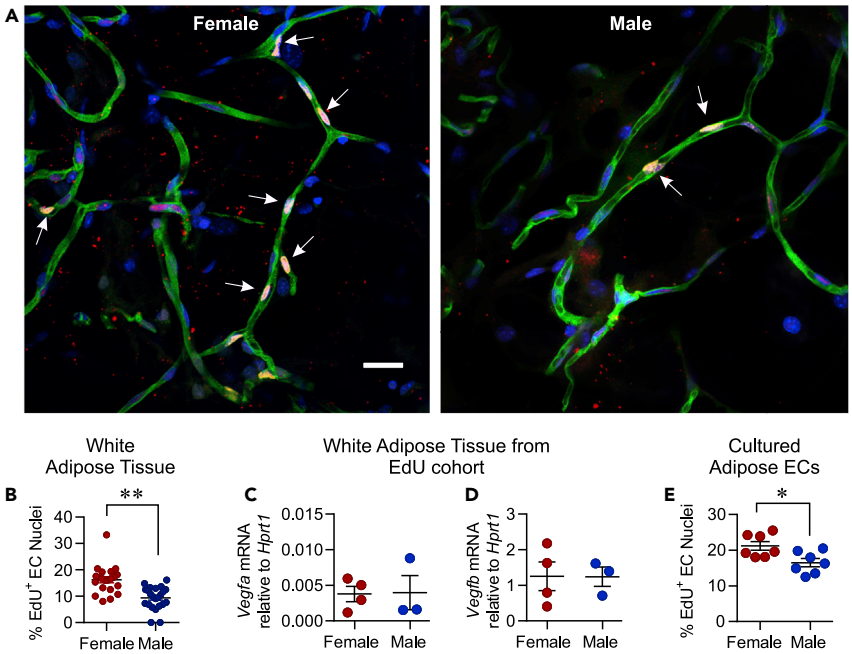

Figure 3. Female adipose EC exhibit elevated proliferation rates compared to male EC

(A and B) Female and male mice were fed an HFD for 7 weeks. EdU was injected two sequential days prior to tissue extraction.

(A) Whole-mount confocal imaging of white visceral adipose tissue to detect proliferating EC. Green (*Griffonia simplicifolia*-FITC), capillaries; Blue (DAPI), nuclei; Red (ERG), Endothelial cell nuclei; Yellow (EdU), proliferating cells. Arrows point to EdU-positive endothelial cell nuclei. Scale bar = 25 μm.

(B) Quantification of EdU-positive EC (ERG+) relative to the total number of EC per field of view. Data points represent individual fields of view from 4 female and 3 male mice. Bars represent mean ± SEM **p = 0.0037, two-tailed unpaired Student's *t* test.

(C and D) RNA was extracted from visceral white adipose tissue of the EdU cohort of female and male mice (n = 4 and 3 respectively). Expression levels of *Vegfa* (C) and *Vegfb* (D) relative to *Hprt1* were quantified by qPCR. Also, refer to Figure S3.

(E) Adipose EC from young, healthy female and male mice were isolated and cultured under growth conditions. Proliferation was assessed by EdU incorporation. EdU-positive cells were quantified as a percentage of total EC number. n = 7 independent experiments/sex; *p = 0.015, two-tailed unpaired Student's *t* test.

EC RNA-Seq analysis (Figure S3A). Transcript levels of leptin, which also exerts pro-angiogenic effects,[23] were higher in the adipose of males compared to females (Figure S3B). This suggests that the augmented proliferation of female EC may be independent of differential levels of angiogenic factors present in the microenvironment. *In vitro* studies employing primary cultures of EC (isolated from the adipose tissue of matched sets of young, healthy male and female mice) also demonstrated a greater proliferative capacity of female EC as detected by EdU incorporation (Figure 3E). Altogether, these experiments reinforce the idea that sex differences in EC proliferation may reflect cell-autonomous differences rather than distinctions in the adipose microenvironment.

Sex-biased inflammatory state under obesogenic conditions may reflect distinct sensitivity of male and female adipose endothelial cells to an inflammatory stimulus

Further characterization was also conducted on the predominant transcriptional phenotype detected in adipose male EC under HFD conditions. In association with their pro-inflammatory profile, male EC displayed significant enrichment of genes belonging to inflammasome and inflammasome assembly gene ontologies (Figures 4A and S4). Considering that the pronounced pro-inflammatory profile of adipose EC from male HF-fed mice can be an indicator of cellular senescence,[24,25] we assessed if hallmark genes associated with senescent cellular behavior were enriched in male versus female EC. Notably, we found that senescence-associated secretory phenotype (SASP)-related genes were enriched in the male adipose EC (Figure 4A and Table S5).

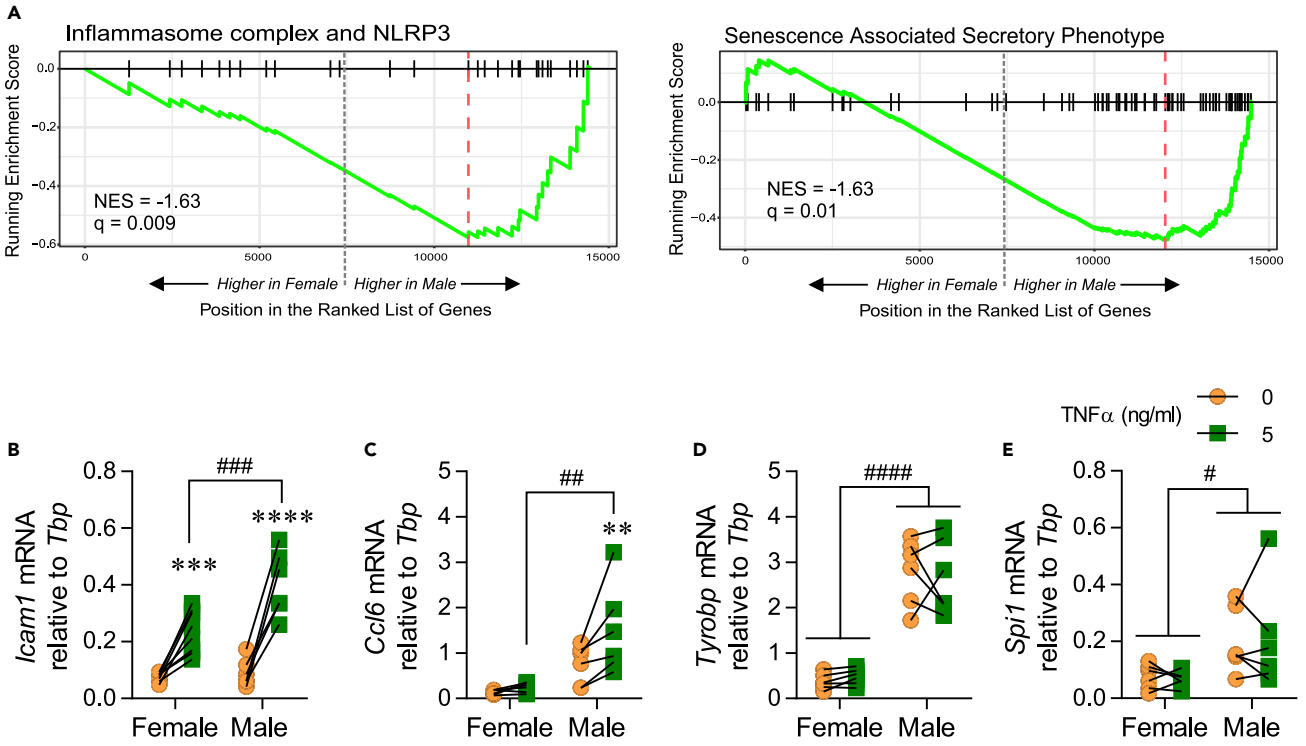

Figure 4. Male adipose EC display an inflammatory profile *in vivo* and *in vitro*

(A) GSEA plots of genes represented in the Inflammasome Complex (GO:0061702) and NLRP3 Inflammasome Complex Assembly (GO:0044546) gene ontologies and SASP-related genes. Corresponding heatmaps are in Figure S4. See also Figure S5. (B–E) TNFα treatment (5 ng/mL; 20 h) of cultured adipose EC from female and male young, healthy mice. mRNA levels of target genes were assessed by qPCR and expressed relative to housekeeping gene Tbp. Data were assessed by 2-way paired ANOVA (Sex x Treatment) with Sidak's post-hoc comparisons; n = 6 independent experiments for female and male EC.

(B) Icam1 mRNA ***p = 0.0006 vs. 0 ng/mL; ****p < 0.0001 vs. 0 ng/mL; ### Interaction Male vs. Female, 5 ng/mL, p = 0.0003.

(C) Ccl6 mRNA **p = 0.0071 vs. 0 ng/mL; ## Interaction Male vs. Female, 5 ng/mL, p = 0.0014.

(D) Tyrobp mRNA ####p < 0.0001 Male vs. Female, for both 0 and 5 ng/mL.

(E) Spi1 mRNA #Main effect of sex, p = 0.045 Male vs. Female. Analyses of additional genes are in Figure S6.

We considered that the greater pro-inflammatory state of the male EC could result from differences in the local adipose microenvironment. However, we did not detect sex differences in the mRNA levels of key inflammatory cytokines *Tnfa* and *Il1b* within the white adipose samples that were used for the EC RNA-Seq analysis (Figure S5). This suggests that the greater pro-inflammatory state of male EC may not be triggered by the differential levels of these cytokines in the white adipose microenvironment. We sought further insight by assessing if sex differences in genes associated with inflammatory responsiveness remained detectable in primary cultures of adipose EC following TNFα stimulation. We examined the transcripts of multiple inflammation or immune-related genes detected as DEGs in our dataset that have also been previously reported to be expressed in mouse microvascular ECs from multiple organs.[26] Multiple acute-response inflammatory genes displayed a sex bias in responsiveness to TNFα. *Icam1* mRNA increased in both sexes with TNFα exposure, but this effect was significantly higher in male versus female EC (interaction between sex and treatment) (Figure 4B). This concurs with a report that ICAM1 expression and leukocyte adherence were lower in mesenteric microvessels of females compared to male mice.[27] Transcript levels of the cytokines *Ccl6* and *Tnf* also displayed an interaction between sex and treatment, increasing in male but not female EC in response to TNFα (Figures 4C and S6). Multiple immune-related genes displayed a significantly greater expression in the male compared to female EC, but no responsiveness to TNFα treatment. This pattern was observed for *Tyrobp*, an immune-modulatory adaptor protein, the transcriptional regulator *Spi1* (Figures 4B and 4C) as well as inflammatory markers *Cd68*, *Ptprc*, and *Itgax* (Figure S6). Together, these data indicate that male adipose ECs display a slightly pro-inflammatory profile under basal conditions and they have greater sensitivity to an inflammatory stimulus.

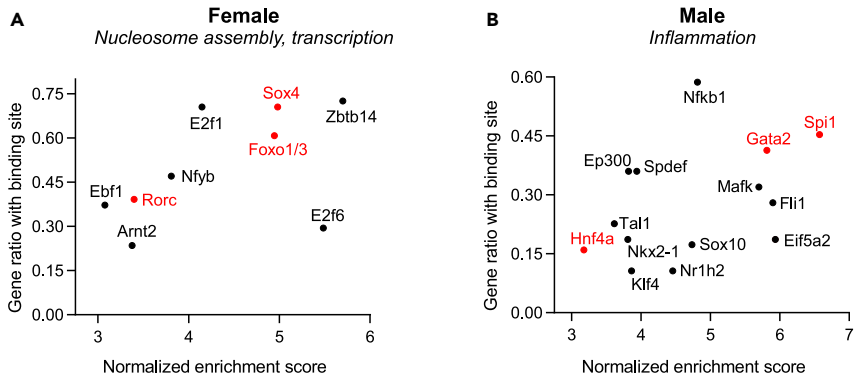

Figure 5. Predicted transcription factors associated with dominant female and male enriched ontologies

iRegulon was used to predict putative transcriptional regulators of female DEGs related to nucleosome assembly and positive regulation of transcription and male DEGs related to the immune system process, inflammatory response, phagocytosis, neutrophil chemotaxis, and antigen processing and presentation. Scatterplots of resultant analyses are shown for female (A) and male (B), in which the X axis indicates the normalized enrichment score (NES) for a given transcription factor and the Y axis shows the ratio of the genes associated with that factor relative to all inputted genes. Red font indicates transcription factors that were also significantly upregulated in that sex.

Transcriptional regulators involved in the proliferative and pro-inflammatory profiles of endothelial cells

Having established the distinct cellular phenotypes of male and female adipose EC, we considered putative transcription factors that might predict the sex-dimorphic endothelial profiles under HFD feeding. The analysis identified several enriched motifs (NES>3) associated with transcription factors and revealed *Zbtb14; E2f6/E2f1; Sox4 and Foxo1/3* as the top predicted regulators of the DEGs associated with ontologies "chromatin/transcription" in female EC. Of these transcription factors, gene expression of *Sox4*, *Foxo1, and Foxo3* mRNA were significantly higher in EC from female HF-fed mice (−1.83, −0.63, and −0.77 logFC, respectively; Figure 5A). Interestingly, estrogen receptor binding sites were not identified amongst the top enriched transcription factor motifs for these transcripts. This corroborates a previous report that estrogen signaling accounts for only a portion of sex differences in gene expression.[28]

Conversely, putative transcriptional regulators that may regulate the male DEGs belonging to "immune response/inflammation" related gene ontologies included *Spi1; Gata2; Fli1; Nfkb1* (Figure 5B). Of these transcription factors, *Spi1* and *Gata2* mRNA were significantly higher in the EC from male HF-fed mice (1.58 and 0.9 logFC, respectively, vs. female EC). *Spi1* and *Gata2* were recently described as putative regulators of an immune response program in EC.[29] Notably, *Spi1*, which has been associated with cellular senescence,[30] was elevated in male compared to female EC from the validation cohort of mice (Table S4) and in cultured cells (Figure 4E).

The sex differences observed in adipose endothelial cells under high-fat diet conditions are also detectable in aged endothelial cells

We sought to corroborate and extend the sex-biased transcriptional profiles revealed in our analysis of EC from HF-fed mice by comparing to an independent transcriptional profile of EC in a different pathophysiological context. Considering the SASP phenotype observed in the male EC, we chose to compare our findings to the transcriptomic signature of EC from several organs (including fat) from aged male and female mice, which was generated utilizing Tabula Muris senis single-cell sequencing data from 18-month-old mice. Overall, males and females exhibit differential patterns of aging.[31] Although it is well-documented that microvascular disease and EC dysfunction increase substantially with aging,[32] sex differences in aging EC and the impact on capillary content remain poorly characterized. We used GSEA to first identify GO BPs associated with the sex-biased gene sets in each dataset independently. The male-biased BPs (220 and 141 in the HFD and aged EC datasets, respectively) were dominantly clustered in ontologies related to "Immune regulation," "migration/chemotaxis," and "Interleukin production" (Table S6). There were 35 identical ontologies displaying male-biased expression in both datasets. Selected ontologies (and their core enrichment genes) that were common between the HFD and aged

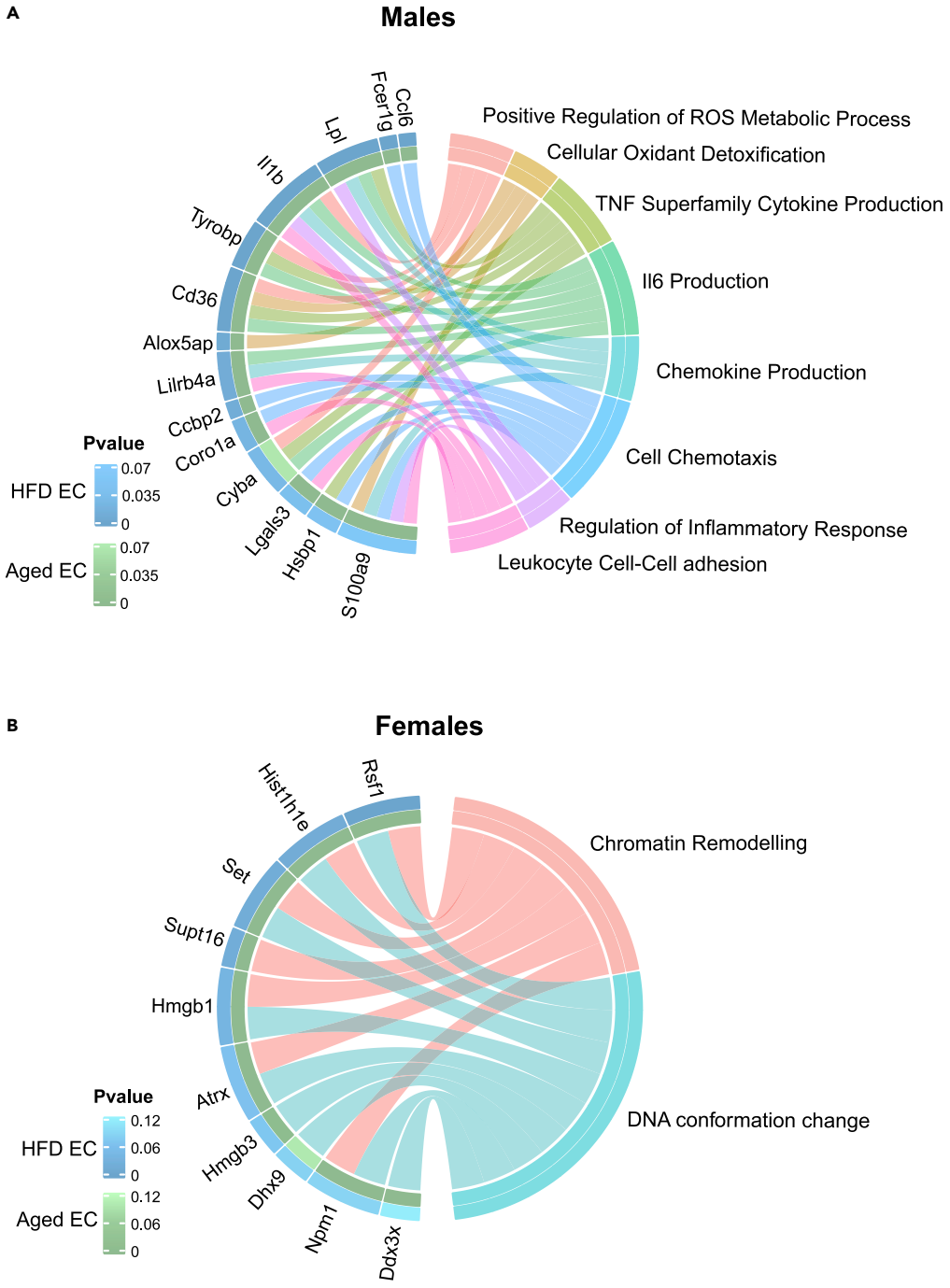

Figure 6. Sex-biased Biological Process ontologies and constituent genes in common between EC from HFD-fed and aged mice

GSEA was used to identify sex-biased GO BPs enriched in EC from both HFD-fed and aged mice. The full analysis is in Table S6. Selected genes belonging to the core enrichment of BPs higher in male EC (A) and in female EC (B) are illustrated by chord plot. For individual genes, the outer ring (blue) represents the adjusted p value of that gene in the HFD RNA-seq dataset and inner ring (green) represents log FC of the gene in the aged mouse dataset (Huang et al., 2021).

EC datasets are displayed in Figure 6A. Conversely, 73 and 40 BPs were female-biased in HFD and aged EC datasets, respectively. Of these, the two major clusters shared between both datasets were associated with DNA organization/conformation and chromatin remodeling (Figure 6B).

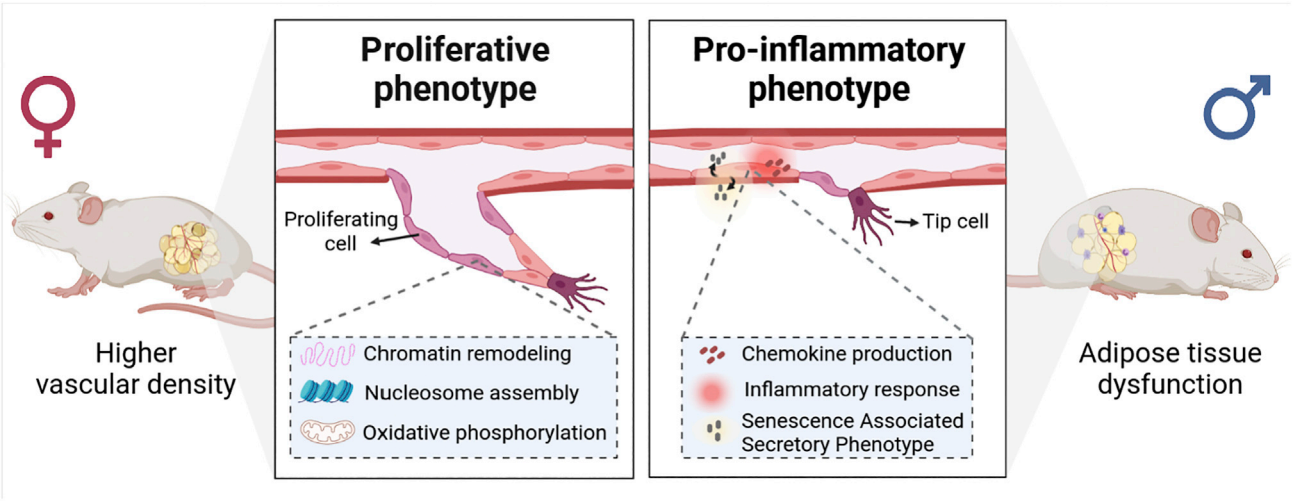

Figure 7. Summary Schematic

Visual representation of key sex-biased BPs identified by the analysis of genes that were differentially expressed in female versus male adipose ECs under obesogenic conditions. These transcriptional signatures may underlie the divergent angiogenic capacities previously reported within white adipose tissue of male and female high-fat diet-fed mice and sex disparities in pathophysiological responses to obesity.

We further tested if the transcriptomes of young healthy EC from 3-month-old mice[33,34] display similar sex-biases as seen in the EC from HFD-fed mice. However, biological pathways enriched in DEG higher in young male (vs female) EC clustered substantially with "vasculogenesis" rather than inflammation (Table S6), consistent with a healthy EC phenotype. Notably, EC from young female mice were enriched in ontologies related to ATP synthesis (oxidative phosphorylation) and ribosomal processes, which more closely paralleled the gene sets enriched in EC of HFD-fed female mice. In sum, these comparisons suggest that HFD and aging evoke similar detrimental effects on male EC whereas EC from female mice appear to resist these deleterious alterations.

DISCUSSION

Herein, we revealed distinct molecular signatures in male and female EC from white adipose tissue of mice upon 7 weeks of HFD feeding (Figure 7). Female adipose EC exhibit a transcriptomic signature associated with a predominantly proliferative state, which manifests as a greater proliferative capacity when compared to male EC. Conversely, EC from male counterparts show enrichment in gene sets involved in a pro-inflammatory phenotype, which seems to be triggered in response to the diet but also affected by differential sensitivity to inflammatory stimuli when compared to female EC. These findings suggest that molecular disparities in EC account, at least in part, for the sex-biased adipose tissue angiogenesis under obesogenic conditions.

The enrichment in proliferation-related genes and elevated EdU incorporation in female EC compared to male counterparts demonstrate that female EC retain the capacity to undergo angiogenesis and expand the local vasculature to meet physiological tissue demands even after several weeks of HFD. This is coherent with the prior observation that adipose vascularization is greater in female compared to male mice after 16 weeks of HFD.[20] In the current study, the similar adipose tissue levels of growth factors (i.e. VEGFA, VEGFB) in both sexes and the proliferative advantage detected in cultured female EC imply that this is a cell-autonomous phenotype. Enrichment of transcripts associated with chromatin modifiers was observed in female adipose EC, suggesting that epigenetic regulatory mechanisms maintain the increased proliferation rate in female EC. These findings fit with a growing body of data documenting a higher proliferation of HUVEC and pulmonary artery EC isolated from female compared to male donors.[16,35] The contrasting ontologies representing both positive and negative regulation of angiogenesis enriched in the male adipose EC suggests that the inhibition of angiogenic signaling in males may lower the proliferative potential of male EC under HFD conditions. The elevated levels of typical "tip cell" marker genes in the male EC appear to concur with this outcome, as proliferation is repressed in tip cells.[36] Interestingly, elevated proliferative activity EC was reported in male mice fed an HFD for just two weeks (but not

after five or fifteen weeks),[37] indicating that HFD may elicit an initial angiogenic response in adipose male EC but that sustained HFD suppresses their proliferative capacity.

Previous studies have established the paradigm that sustained HFD dysregulates critical EC cellular signaling pathways, inducing oxidative stress, inflammation, and senescence.[6–8,38,39] The overt inflammatory signature prevalent in the male adipose EC in our study provides evidence of EC dysfunction,[1] agreeing with this established paradigm. The development of inflammation may underlie the enrichment of negative regulators of angiogenesis and the senescence-associated signature (SASP) displayed by the male adipose EC. In turn, these molecular signatures likely contribute to the poor angiogenic response observed in the adipose of male mice during long-term HFD. Of note, SASP is a hallmark of aged or damaged cells that can exert deleterious effects on surrounding cells[40] and may contribute to the sex-biased development of adipose tissue dysfunction with obesity. Considering that higher levels of inflammatory cytokines similar to the ones observed in our work were recently reported in male EC from obese compared to lean mice following 18 weeks of HFD, it is probable that the inflammatory profile of male EC in our study is largely induced by the diet.[39] The pro-inflammatory signature in the transcriptome of adipose EC from male HFD-fed mice also was in common with those detected in EC from aged male mice, which concurs with reports that EC dysfunction and inflammation generally manifests at an earlier age in males than females.[41,42]

Our findings that female EC did not develop the same extent of inflammation as seen in the male adipose EC, and instead retained proliferative capacity, suggests a higher resistance of female EC to the stress associated with prolonged HFD. This corroborates several reports showing that cultured female EC exhibited higher viability than male EC when challenged with serum starvation, hyperoxia, shear stress, or oxidative stress.[18,19] One plausible contributor to their stress tolerance is the enrichment in genes involved in the electron transport chain in female compared to male adipose EC. This sex-biased pattern of gene expression, also detected in the EC from healthy young mice, has been reported across numerous cell types and species.[28,43,44] Indeed, higher oxidative phosphorylation gene content is linked with greater stress resistance and longevity[45,46] whereas the lower mitochondrial content in the adipose of males has been associated with a greater risk of developing metabolic dysfunction.[43]

There is growing awareness that EC express immune-related transcripts and can play tissue-specific immune-modulatory roles.[47] In addition to the diet effect on inflammatory genes, we found that male adipose EC in culture exhibited higher basal levels of some immune response-related genes than female EC and greater responsiveness to TNFα-stimulated conditions. This suggests a sustained distinction between male and female EC that is not dependent on immediate cues from the environment, which is in line with recent work demonstrating that epigenetic encoding of chromatin accessibility plays a critical role in establishing immune response potential.[29] Therefore, it is likely that the EC dysfunction of male adipose ECs results not only from lower resistance to stress but also because of a greater inherent responsiveness to an inflammatory stimulus, which may divert these cells from an angiogenic response under obesogenic conditions. We propose that epigenetic mechanisms support the underlying sex differences in the EC phenotype of both male and female EC and that these sex differences are amplified by the obesogenic conditions triggered by HFD.

Overall, the distinctive molecular signatures of male and female EC under HFD conditions provide strong support for the concept that sex differences in EC behavior and angiogenesis contribute to the well-described sex disparities in the development of obesity and its related complications. This indicates that the male overrepresentation in prior studies has generated an incomplete understanding of the factors impacting vascular remodeling during adipose tissue expansion. Our results suggest that female EC have a better capacity to cope with the stress imposed by HFD. These phenotypic differences may also apply to other conditions such as aging. Thus, this study opens new perspectives on the influence of sex in the pathophysiology of EC in obesity and emphasizes the importance of considering sex as a significant variable in the regulation of vascular remodeling and the contribution of EC in disease states.

Limitations of the study

This study was designed to understand molecular mechanisms underlying the greater adipose angiogenesis observed in HFD-fed female versus male mice rather than to study how HFD-feeding alters the transcriptome of male and female adipose EC. Comparison with publicly available datasets from standard diet-fed mice combined with the gene expression analysis of cultured EC allowed us to infer that the extent

of inflammation in the male EC was in part induced by HFD. However, future studies should extend this observation by directly assessing the impact of diet on the EC molecular signatures in both sexes. The relative contributions of the gonadal hormones and genes localized to the Y chromosome to the observed sex-biased EC phenotypes remain undefined, requiring further investigation. Our study relied on the tissue dissociation and isolation of EC using a magnetic bead-based enrichment protocol. While *in vitro* approaches employed in our study alongside the comparison of other publicly available EC databases provide the support that the major molecular signatures presented in this article reflect those of EC, we cannot completely exclude the possibility of low-level contamination of the RNA by other cell types as well as the loss of EC during isolation. Future studies combining spatially resolved transcriptional profiling with single-cell RNA sequencing can provide greater insight into distinct EC sub-populations that might be altered by sex or by diet. Exploration of these EC sex differences within human adipose will be important in advancing the health-related implications of our study.

STAR★METHODS

Detailed methods are provided in the online version of this paper and include the following:

- KEY RESOURCES TABLE
- RESOURCE AVAILABILITY
  - Lead contact
  - Materials availability
  - Data and code availability
- EXPERIMENTAL MODEL AND SUBJECT DETAILS
  - Mice
  - Primary murine endothelial cell cultures
- METHOD DETAILS
  - Adipose EC isolation for RNA seq
  - Bulk RNA seq
  - Gene ontology and set enrichment analyses
  - Bioinformatic inference of transcriptional regulators
  - Comparison with publicly available EC data
  - Whole-mount imaging of adipose tissue
  - *In vitro* proliferation assays
  - *In vitro* TNFα stimulation
  - RNA analysis by qPCR
  - Western Blot analysis
- QUANTIFICATION AND STATISTICAL ANALYSES

SUPPLEMENTAL INFORMATION

Supplemental information can be found online at https://doi.org/10.1016/j.isci.2022.105811.

ACKNOWLEDGMENTS

The authors thank Mr. Daniel Stueckmann for the discussion of bioinformatics analyses and R code support, and Dr. Anthony Scimè for critical reading of the article. The visual abstract and schematic figure were created with Biorender.com. This work was supported by Canadian Institutes of Health Research project grant (#MOP-130491; TLH and ERo) and by Natural Science and Engineering Researches Council of Canada Discovery grant (#RGPIN-2018-05858; TLH) and York University Faculty of Health minor research grant (TLH).

AUTHOR CONTRIBUTIONS

Conceptualization: MR, AP, ERo, TH; investigation: MR, AP, OR, AF, EN, and TH. Bioinformatics analyses: ERu, AP; sample preparation and analysis: MR, AP, OR, ERo, TG, and TH . Writing: MR, AP, and TH, with contributions from all authors. Visualization: MR, AP, and TH; project administration: TH; funding acquisition: ERo and TH.

DECLARATION OF INTERESTS

The authors declare no competing interests.

Received: August 29, 2022
Revised: November 13, 2022
Accepted: December 9, 2022
Published: January 20, 2023

REFERENCES

1. Pober, J.S., and Sessa, W.C. (2007). Evolving functions of endothelial cells in inflammation. Nat. Rev. Immunol. *7*, 803–815. https://doi.org/10.1038/nri2171.

2. Augustin, H.G., and Koh, G.Y. (2017). Organotypic vasculature: from descriptive heterogeneity to functional pathophysiology. Science *357*, eaal2379. https://doi.org/10.1126/science.aal2379.

3. Potente, M., and Carmeliet, P. (2017). The link between angiogenesis and endothelial metabolism. Annu. Rev. Physiol. *79*, 43–66. https://doi.org/10.1146/annurev-physiol-021115-105134.

4. Geudens, I., and Gerhardt, H. (2011). Coordinating cell behaviour during blood vessel formation. Development *138*, 4569–4583. https://doi.org/10.1242/dev.062323.

5. Corvera, S., and Gealekman, O. (2014). Adipose tissue angiogenesis: impact on obesity and type-2 diabetes. Biochim. Biophys. Acta *1842*, 463–472. https://doi.org/10.1016/j.bbadis.2013.06.003.

6. Aoqui, C., Chmielewski, S., Scherer, E., Eissler, R., Sollinger, D., Heid, I., Braren, R., Schmaderer, C., Megens, R.T., Weber, C., et al. (2014). Microvascular dysfunction in the course of metabolic syndrome induced by high-fat diet. Cardiovasc. Diabetol. *13*, 31. https://doi.org/10.1186/1475-2840-13-31.

7. García-Prieto, C.F., Hernández-Nuño, F., Rio, D.D., Ruiz-Hurtado, G., Aránguez, I., Ruiz-Gayo, M., Somoza, B., and Fernández-Alfonso, M.S. (2015). High-fat diet induces endothelial dysfunction through a down-regulation of the endothelial AMPK-PI3K-Akt-eNOS pathway. Mol. Nutr. Food Res. *59*, 520–532. https://doi.org/10.1002/mnfr.201400539.

8. Molnar, J., Yu, S., Mzhavia, N., Pau, C., Chereshnev, I., and Dansky, H.M. (2005). Diabetes induces endothelial dysfunction but does not increase neointimal formation in high-fat diet fed C57BL/6J mice. Circ. Res. *96*, 1178–1184. https://doi.org/10.1161/01.RES.0000168634.74330.

9. Rudnicki, M., Abdifarkosh, G., Nwadozi, E., Ramos, S.V., Makki, A., Sepa-Kishi, D.M., Ceddia, R.B., Perry, C.G., Roudier, E., and Haas, T.L. (2018). Endothelial-specific FoxO1 depletion prevents obesity-related disorders by increasing vascular metabolism and growth. Elife *7*, e39780. https://doi.org/10.7554/eLife.39780.

10. Sung, H.-K., Doh, K.-O., Son, J.E., Park, J.G., Bae, Y., Choi, S., Nelson, S.M.L., Cowling, R., Nagy, K., Michael, I.P., et al. (2013). Adipose vascular endothelial growth factor regulates metabolic homeostasis through angiogenesis. Cell Metabol. *17*, 61–72. https://doi.org/10.1016/j.cmet.2012.12.010.

11. Robciuc, M.R., Kivelä, R., Williams, I.M., de Boer, J.F., van Dijk, T.H., Elamaa, H., Tigistu-Sahle, F., Molotkov, D., Leppänen, V.M., Käkelä, R., et al. (2016). VEGFB/VEGFR1-Induced expansion of adipose vasculature counteracts obesity and related metabolic complications. Cell Metabol. *23*, 712–724. https://doi.org/10.1016/j.cmet.2016.03.004.

12. Goossens, G.H., Jocken, J.W.E., and Blaak, E.E. (2021). Sexual dimorphism in cardiometabolic health: the role of adipose tissue, muscle and liver. Nat. Rev. Endocrinol. *17*, 47–66. https://doi.org/10.1038/s41574-020-00431-8.

13. Yoon, D.Y., Mansukhani, N.A., Stubbs, V.C., Helenowski, I.B., Woodruff, T.K., and Kibbe, M.R. (2014). Sex bias exists in basic science and translational surgical research. Surgery *156*, 508–516. https://doi.org/10.1016/j.surg.2014.07.001.

14. Zucker, I., and Beery, A.K. (2010). Males still dominate animal studies. Nature *465*, 690. https://doi.org/10.1038/465690a.

15. Hartman, R.J.G., Kapteijn, D.M.C., Haitjema, S., Bekker, M.N., Mokry, M., Pasterkamp, G., Civelek, M., and den Ruijter, H.M. (2020). Intrinsic transcriptomic sex differences in human endothelial cells at birth and in adults are associated with coronary artery disease targets. Sci. Rep. *10*, 12367. https://doi.org/10.1038/s41598-020-69451-8.

16. Addis, R., Campesi, I., Fois, M., Capobianco, G., Dessole, S., Fenu, G., Montella, A., Cattaneo, M.G., Vicentini, L.M., and Franconi, F. (2014). Human umbilical endothelial cells (HUVECs) have a sex: characterisation of the phenotype of male and female cells. Biol. Sex Differ. *5*, 18. https://doi.org/10.1186/s13293-014-0018-2.

17. Cattaneo, M.G., Vanetti, C., Decimo, I., Di Chio, M., Martano, G., Garrone, G., Bifari, F., and Vicentini, L.M. (2017). Sex-specific eNOS activity and function in human endothelial cells. Sci. Rep. *7*, 9612. https://doi.org/10.1038/s41598-017-10139-x.

18. Lorenz, M., Koschate, J., Kaufmann, K., Kreye, C., Mertens, M., Kuebler, W.M., Baumann, G., Gossing, G., Marki, A., Zakrzewicz, A., et al. (2015). Does cellular sex matter? Dimorphic transcriptional differences between female and male endothelial cells. Atherosclerosis *240*, 61–72. https://doi.org/10.1016/j.atherosclerosis.2015.02.018.

19. Lorenz, M., Blaschke, B., Benn, A., Hammer, E., Witt, E., Kirwan, J., Fritsche-Guenther, R., Gloaguen, Y., Bartsch, C., Vietzke, A., et al. (2019). Sex-specific metabolic and functional differences in human umbilical vein endothelial cells from twin pairs. Atherosclerosis *291*, 99–106. https://doi.org/10.1016/j.atherosclerosis.2019.10.007.

20. Rudnicki, M., Abdifarkosh, G., Rezvan, O., Nwadozi, E., Roudier, E., and Haas, T.L. (2018). Female mice have higher angiogenesis in perigonadal adipose tissue than males in response to high-fat diet. Front. Physiol. *9*, 1452. https://doi.org/10.3389/fphys.2018.01452.

21. De Bock, K., Georgiadou, M., Schoors, S., Kuchnio, A., Wong, B.W., Cantelmo, A.R., Quaegebeur, A., Ghesquière, B., Cauwenberghs, S., Eelen, G., et al. (2013). Role of PFKFB3-driven glycolysis in vessel sprouting. Cell *154*, 651–663. https://doi.org/10.1016/j.cell.2013.06.037.

22. Diebold, L.P., Gil, H.J., Gao, P., Martinez, C.A., Weinberg, S.E., and Chandel, N.S. (2019). Mitochondrial complex III is necessary for endothelial cell proliferation during angiogenesis. Nat. Metab. *1*, 158–171. https://doi.org/10.1038/s42255-018-0011-x.

23. Sierra-Honigmann, M.R., Nath, A.K., Murakami, C., García-Cardeña, G., Papapetropoulos, A., Sessa, W.C., Madge, L.A., Schechner, J.S., Schwabb, M.B., Polverini, P.J., and Flores-Riveros, J.R. (1998). Biological action of leptin as an angiogenic factor. Science *281*, 1683–1686. https://doi.org/10.1126/science.281.5383.1683.

24. Spinelli, R., Parrillo, L., Longo, M., Florese, P., Desiderio, A., Zatterale, F., Miele, C., Raciti, G.A., and Beguinot, F. (2020). Molecular basis of ageing in chronic metabolic diseases. J. Endocrinol. Invest. *43*, 1373–1389. https://doi.org/10.1007/s40618-020-01255-z.

25. Tchkonia, T., Morbeck, D.E., Von Zglinicki, T., Van Deursen, J., Lustgarten, J., Scrable, H., Khosla, S., Jensen, M.D., and Kirkland, J.L. (2010). Fat tissue, aging, and cellular senescence. Aging Cell *9*, 667–684. https://doi.org/10.1111/j.1474-9726.2010.00608.x.

26. Jambusaria, A., Hong, Z., Zhang, L., Srivastava, S., Jana, A., Toth, P.T., Dai, Y., Malik, A.B., and Rehman, J. (2020). Endothelial heterogeneity across distinct vascular beds during homeostasis and inflammation. Elife *9*, e51413. https://doi.org/10.7554/eLife.51413.

27. Moss, M.E., Lu, Q., Iyer, S.L., Engelbertsen, D., Marzolla, V., Caprio, M., Lichtman, A.H., and Jaffe, I.Z. (2019). Endothelial mineralocorticoid receptors contribute to vascular inflammation in atherosclerosis in a sex-specific manner. Arterioscler. Thromb. Vasc. Biol. *39*, 1588–1601. https://doi.org/10.1161/ATVBAHA.119.312954.

28. Lopes-Ramos, C.M., Chen, C.-Y., Kuijjer, M.L., Paulson, J.N., Sonawane, A.R., Fagny, M.,

Platig, J., Glass, K., Quackenbush, J., and DeMeo, D.L. (2020). Sex differences in gene expression and regulatory networks across 29 human tissues. Cell Rep. *31*, 107795. https://doi.org/10.1016/j.celrep.2020.107795.

29. Krausgruber, T., Fortelny, N., Fife-Gernedl, V., Senekowitsch, M., Schuster, L.C., Lercher, A., Nemc, A., Schmidl, C., Rendeiro, A.F., Bergthaler, A., and Bock, C. (2020). Structural cells are key regulators of organ-specific immune responses. Nature *583*, 296–302. https://doi.org/10.1038/s41586-020-2424-4.

30. Delestré, L., Cui, H., Esposito, M., Quiveron, C., Mylonas, E., Penard-Lacronique, V., Bischof, O., and Guillouf, C. (2017). Senescence is a Spi1-induced anti-proliferative mechanism in primary hematopoietic cells. Haematologica *102*, 1850–1860. https://doi.org/10.3324/haematol.2016.157636.

31. Hägg, S., and Jylhävä, J. (2021). Sex differences in biological aging with a focus on human studies. Elife *10*, e63425. https://doi.org/10.7554/eLife.63425.

32. Donato, A.J., Machin, D.R., and Lesniewski, L.A. (2018). Mechanisms of dysfunction in the aging vasculature and role in age-related disease. Circ. Res. *123*, 825–848. https://doi.org/10.1161/CIRCRESAHA.118.312563.

33. Huang, X., Shen, W., Veizades, S., Liang, G., Sayed, N., and Nguyen, P.K. (2021). Single-cell transcriptional profiling reveals sex and age diversity of gene expression in mouse endothelial cells. Front. Genet. *12*, 590377. https://doi.org/10.3389/fgene.2021.590377.

34. Schaum, N., Lehallier, B., Hahn, O., Pálovics, R., Hosseinzadeh, S., Lee, S.E., Sit, R., Lee, D.P., Losada, P.M., Zardeneta, M.E., et al. (2020). Ageing hallmarks exhibit organ-specific temporal signatures. Nature *583*, 596–602. https://doi.org/10.1038/s41586-020-2499-y.

35. Qin, S., Predescu, D.N., Patel, M., Drazkowski, P., Ganesh, B., and Predescu, S.A. (2020). Sex differences in the proliferation of pulmonary artery endothelial cells: implications for plexiform arteriopathy. J. Cell Sci. *133*, jcs237776. https://doi.org/10.1242/jcs.237776.

36. Gerhardt, H., Golding, M., Fruttiger, M., Ruhrberg, C., Lundkvist, A., Abramsson, A., Jeltsch, M., Mitchell, C., Alitalo, K., Shima, D., and Betsholtz, C. (2003). VEGF guides angiogenic sprouting utilizing endothelial tip cell filopodia. J. Cell Biol. *161*, 1163–1177. https://doi.org/10.1083/jcb.200302047.

37. Voros, G., Maquoi, E., Demeulemeester, D., Clerx, N., Collen, D., and Lijnen, H.R. (2005). Modulation of angiogenesis during adipose tissue development in murine models of obesity. Endocrinology *146*, 4545–4554. https://doi.org/10.1210/en.2005-0532.

38. Wang, C.-Y., Kim, H.-H., Hiroi, Y., Sawada, N., Salomone, S., Benjamin, L.E., Walsh, K., Moskowitz, M.A., and Liao, J.K. (2009). Obesity increases vascular senescence and susceptibility to ischemic injury through chronic activation of akt and mTOR. Sci. Signal. *2*, ra11. https://doi.org/10.1126/scisignal.2000143.

39. Sárvári, A.K., Van Hauwaert, E.L., Markussen, L.K., Gammelmark, E., Marcher, A.-B., Ebbesen, M.F., Nielsen, R., Brewer, J.R., Madsen, J.G.S., and Mandrup, S. (2021). Plasticity of epididymal adipose tissue in response to diet-induced obesity at single-nucleus resolution. Cell Metabol. *33*, 437–453.e5. https://doi.org/10.1016/j.cmet.2020.12.004.

40. Rodier, F., Coppé, J.P., Patil, C.K., Hoeijmakers, W.A.M., Muñoz, D.P., Raza, S.R., Freund, A., Campeau, E., Davalos, A.R., and Campisi, J. (2009). Persistent DNA damage signalling triggers senescence-associated inflammatory cytokine secretion. Nat. Cell Biol. *11*, 973–979. https://doi.org/10.1038/ncb1909.

41. Celermajer, D.S., Sorensen, K.E., Spiegelhalter, D.J., Georgakopoulos, D., Robinson, J., and Deanfield, J.E. (1994). Aging is associated with endothelial dysfunction in healthy men years before the age-related decline in women. J. Am. Coll. Cardiol. *24*, 471–476. https://doi.org/10.1016/0735-1097(94)90305-0.

42. Cole, J.A., Kehmeier, M.N., Bedell, B.R., Krishna Kumaran, S., Henson, G.D., and Walker, A.E. (2022). Sex differences in the relation between frailty and endothelial dysfunction in old mice. J. Gerontol. A Biol. Sci. Med. Sci. *77*, 416–423. https://doi.org/10.1093/gerona/glab317.

43. Norheim, F., Hasin-Brumshtein, Y., Vergnes, L., Chella Krishnan, K., Pan, C., Seldin, M.M., Hui, S.T., Mehrabian, M., Zhou, Z., Gupta, S., et al. (2019). Gene-by-Sex interactions in mitochondrial functions and cardio-metabolic traits. Cell Metabol. *29*, 932–949.e4. https://doi.org/10.1016/j.cmet.2018.12.013.

44. Chella Krishnan, K., Vergnes, L., Acín-Pérez, R., Stiles, L., Shum, M., Ma, L., Mouisel, E., Pan, C., Moore, T.M., Péterfy, M., et al. (2021). Sex-specific genetic regulation of adipose mitochondria and metabolic syndrome by Ndufv2. Nat. Metab. *3*, 1552–1568. https://doi.org/10.1038/s42255-021-00481-w.

45. Kristensen, T.N., Loeschcke, V., Tan, Q., Pertoldi, C., and Mengel-From, J. (2019). Sex and age specific reduction in stress resistance and mitochondrial DNA copy number in Drosophila melanogaster. Sci. Rep. *9*, 12305. https://doi.org/10.1038/s41598-019-48752-7.

46. Magalhaes-Novais, S., Blecha, J., Naraine, R., Mikesova, J., Abaffy, P., Pecinova, A., Milosevic, M., Bohuslavova, R., Prochazka, J., Khan, S., et al. (2022). Mitochondrial respiration supports autophagy to provide stress resistance during quiescence. Autophagy *18*, 2409–2426. https://doi.org/10.1080/15548627.2022.2038898.

47. Amersfoort, J., Eelen, G., and Carmeliet, P. (2022). Immunomodulation by endothelial cells - partnering up with the immune system? Nat. Rev. Immunol. *22*, 576–588. https://doi.org/10.1038/s41577-022-00694-4.

48. Janky, R., Verfaillie, A., Imrichová, H., Van de Sande, B., Standaert, L., Christiaens, V., Hulselmans, G., Herten, K., Naval Sanchez, M., Potier, D., et al. (2014). iRegulon: from a gene list to a gene regulatory network using large motif and track collections. PLoS Comput. Biol. *10*, e1003731. https://doi.org/10.1371/journal.pcbi.1003731.

49. Gu, Z., Gu, L., Eils, R., Schlesner, M., and Brors, B. (2014). Circlize implements and enhances circular visualization in R. Bioinformatics *30*, 2811–2812. https://doi.org/10.1093/bioinformatics/btu393.

50. Shannon, P., Markiel, A., Ozier, O., Baliga, N.S., Wang, J.T., Ramage, D., Amin, N., Schwikowski, B., and Ideker, T. (2003). Cytoscape: a software environment for integrated models of biomolecular interaction networks. Genome Res. *13*, 2498–2504. https://doi.org/10.1101/gr.1239303.

51. Huang, D.W., Sherman, B.T., and Lempicki, R.A. (2009). Bioinformatics enrichment tools: paths toward the comprehensive functional analysis of large gene lists. Nucleic Acids Res. *37*, 1–13. https://doi.org/10.1093/nar/gkn923.

52. Robinson, M.D., McCarthy, D.J., and Smyth, G.K. (2010). edgeR: a Bioconductor package for differential expression analysis of digital gene expression data. Bioinformatics *26*, 139–140. https://doi.org/10.1093/bioinformatics/btp616.

53. Yu, G., and Hu, E. (2019). Enrichplot: Visualization of Functional Enrichment Result.

54. Subramanian, A., Tamayo, P., Mootha, V.K., Mukherjee, S., Ebert, B.L., Gillette, M.A., Paulovich, A., Pomeroy, S.L., Golub, T.R., Lander, E.S., and Mesirov, J.P. (2005). Gene set enrichment analysis: a knowledge-based approach for interpreting genome-wide expression profiles. Proc. Natl. Acad. Sci. USA *102*, 15545–15550. https://doi.org/10.1073/pnas.0506580102.

55. Schneider, C.A., Rasband, W.S., and Eliceiri, K.W. (2012). NIH Image to ImageJ: 25 years of image analysis. Nat. Methods *9*, 671–675. https://doi.org/10.1038/nmeth.2089.

56. Huang, D.W., Sherman, B.T., and Lempicki, R.A. (2009). Systematic and integrative analysis of large gene lists using DAVID bioinformatics resources. Nat. Protoc. *4*, 44–57. https://doi.org/10.1038/nprot.2008.211.

57. Kalluri, A.S., Vellarikkal, S.K., Edelman, E.R., Nguyen, L., Subramanian, A., Ellinor, P.T., Regev, A., Kathiresan, S., and Gupta, R.M. (2019). Single-cell analysis of the normal mouse aorta reveals functionally distinct endothelial cell populations. Circulation *140*, 147–163. https://doi.org/10.1161/CIRCULATIONAHA.118.038362.

58. Goveia, J., Rohlenova, K., Taverna, F., Treps, L., Conradi, L.-C., Pircher, A., Geldhof, V., de Rooij, L.P.M.H., Kalucka, J., Sokol, L., et al. (2020). An integrated gene expression landscape profiling approach to identify lung tumor endothelial cell heterogeneity and angiogenic candidates. Cancer Cell *37*, 21–36.e13. https://doi.org/10.1016/j.ccell.2019.12.001.

59. Li, G., Tian, L., Goodyer, W., Kort, E.J., Buikema, J.W., Xu, A., Wu, J.C., Jovinge, S., and Wu, S.M. (2019). Single cell expression analysis reveals anatomical and cell cycle-dependent transcriptional shifts during heart development. Development *146*. https://doi.org/10.1242/dev.173476.

60. Kalucka, J., de Rooij, L.P.M.H., Goveia, J., Rohlenova, K., Dumas, S.J., Meta, E., Conchinha, N.V., Taverna, F., Teuwen, L.-A., Veys, K., et al. (2020). Single-cell transcriptome atlas of murine endothelial cells. Cell *180*, 764–779.e20. https://doi.org/10.1016/j.cell.2020.01.015.

61. Niethamer, T.K., Stabler, C.T., Leach, J.P., Zepp, J.A., Morley, M.P., Babu, A., Zhou, S., and Morrisey, E.E. (2020). Defining the role of pulmonary endothelial cell heterogeneity in the response to acute lung injury. Elife *9*, e53072. https://doi.org/10.7554/eLife.53072.

62. Orsenigo, F., Conze, L.L., Jauhiainen, S., Corada, M., Lazzaroni, F., Malinverno, M., Sundell, V., Cunha, S.I., Brännström, J., Globisch, M.A., et al. (2020). Mapping endothelial-cell diversity in cerebral cavernous malformations at single-cell resolution. Elife *9*, e61413. https://doi.org/10.7554/eLife.61413.

63. Tombor, L.S., John, D., Glaser, S.F., Luxán, G., Forte, E., Furtado, M., Rosenthal, N., Baumgarten, N., Schulz, M.H., Wittig, J., et al. (2021). Single cell sequencing reveals endothelial plasticity with transient mesenchymal activation after myocardial infarction. Nat. Commun. *12*, 681. https://doi.org/10.1038/s41467-021-20905-1.

64. Coppé, J.P., Patil, C.K., Rodier, F., Sun, Y., Muñoz, D.P., Goldstein, J., Nelson, P.S., Desprez, P.-Y., and Campisi, J. (2008). Senescence-associated secretory phenotypes reveal cell-nonautonomous functions of oncogenic RAS and the p53 tumor suppressor. PLoS Biol. *6*, 2853–2868. https://doi.org/10.1371/journal.pbio.0060301.

65. Basisty, N., Kale, A., Jeon, O.H., Kuehnemann, C., Payne, T., Rao, C., Holtz, A., Shah, S., Sharma, V., Ferrucci, L., et al. (2020). A proteomic atlas of senescence-associated secretomes for aging biomarker development. PLoS Biol. *18*, e3000599. https://doi.org/10.1371/journal.pbio.3000599.

66. Kiss, T., Nyúl-Tóth, Á., Balasubramanian, P., Tarantini, S., Ahire, C., DelFavero, J., Yabluchanskiy, A., Csipo, T., Farkas, E., Wiley, G., et al. (2020). Single-cell RNA sequencing identifies senescent cerebromicrovascular endothelial cells in the aged mouse brain. Geroscience *42*, 429–444. https://doi.org/10.1007/s11357-020-00177-1.

67. Merico, D., Isserlin, R., Stueker, O., Emili, A., and Bader, G.D. (2010). Enrichment map: a network-based method for gene-set enrichment visualization and interpretation. PLoS One *5*, e13984. https://doi.org/10.1371/journal.pone.0013984.

68. Su, G., Kuchinsky, A., Morris, J.H., States, D.J., and Meng, F. (2010). GLay: community structure analysis of biological networks. Bioinformatics *26*, 3135–3137. https://doi.org/10.1093/bioinformatics/btq596.

69. Rudnicki, M., Pislaru, A., and Haas, T.L. (2022). Quantitative methods to assess adipose vasculature. Methods Mol. Biol. *2441*, 201–221. https://doi.org/10.1007/978-1-0716-2059-5_16.

STAR★METHODS

KEY RESOURCES TABLE

REAGENT or RESOURCE	SOURCE	IDENTIFIER
Antibodies		
Mouse monoclonal anti-β-Actin (clone C4)	Santa Cruz Biotechnology	Cat#sc-47778; RRID:AB_626632
Rabbit polyclonal anti-α/β-tubulin	Cell Signaling Technology	Cat#2148; RRID:AB_2288042
Rabbit monoclonal anti-PFKFB3 (clone D7H4Q)	Cell Signalling Technology	Cat#13123; RRID:AB_2617178
Rabbit monoclonal anti-Hexokinase II (clone C64G5)	Cell Signalling Technology	Cat#2867; RRID:AB_2232946
Rabbit monoclonal anti-GAPDH (clone D16H11) XP®	Cell Signalling Technology	Cat#5174; RRID:AB_10622025
Rabbit monoclonal anti-ERG (clone A7L1G)	Cell Signalling Technology	Cat#97249; RRID:AB_2721841
Rat monoclonal anti-mouse CD31, biotin conjugated (clone MEC 13.3)	BD Biosciences	Cat#553371; RRID:AB_394817
Rat monoclonal anti-mouse CD144 (clone 11D4.1)	BD Biosciences	Cat#555289; RRID:AB_395707
Goat polyclonal anti-rabbit IgG, Alexa Fluor® 647 conjugated	Jackson Immunoresearch	Cat#111-605-003; RRID:AB_2338072
Chemicals, peptides, and recombinant proteins		
5-Ethynyl-2′-deoxyuridine	Sigma Aldrich	Cat#900584
Azide-fluor 488	Sigma Aldrich	Cat#760765
Azide-fluor 545	Sigma Aldrich	Cat#760757
Copper(II) sulfate	Sigma Aldrich	Cat#451657
L-Ascorbic acid	Sigma Aldrich	Cat#A7506
Recombinant Murine Tumor Necrosis Factor-alpha	Bio Basic Incorporation	Cat#RC234-12
Critical commercial assays		
RNeasy Mini Kit	Qiagen	Cat#74106
Click-iT™ EdU Imaging Kit	Thermo Fisher Scientific	Cat#C10214
Deposited data		
RNA sequencing data	This paper	NCBI GEO:GSE216585
Tabula Muris Senis gene analysis	Huang et al.[33]	https://doi.org/10.3389/fgene.2021.590377
Experimental models: Cell lines		
Primary mouse adipose endothelial cells	This paper	N/A
Experimental models: Organisms/strains		
Mouse: FVB;B6	York University	N/A
Mouse: C57BL/6J	The Jackson Laboratory	RRID:IMSR_JAX:000664
Oligonucleotides		
See Table S7		
Software and algorithms		
Circlize	https://cran.r-project.org/web/packages/circlize/index.html; Gu et al.[49]	RRID:SCR_002141
Cytoscape	http://cytoscape.org; Shannon et al.[50]	RRID:SCR_003032
DAVID	http://david.abcc.ncifcrf.gov/; Huang et al.[51]	RRID:SCR_001881
EdgeR	http://bioconductor.org/packages/edgeR/; Robinson et al.[52]	RRID:SCR_012802
Enrichplot (R)	https://bioconductor.org/packages/release/bioc/html/enrichplot.html; Yu and Hu[53]	N/A

(Continued on next page)

Continued

REAGENT or RESOURCE	SOURCE	IDENTIFIER
Gene Set Enrichment Analysis	http://www.gsea-msigdb.org/gsea/downloads.jsp; Subramanian et al.[54]	RRID:SCR_003199
GraphPad Prism	http://www.graphpad.com/	RRID:SCR_002798
ImageJ	https://imagej.net/; Schneider et al.[55]	RRID:SCR_003070
Other		
Collagenase, Type I	Thermo Fisher Scientific	Cat#17100017
Collagenase, Type I	Worthington Biochemicals	Cat#LS004197
Dynabeads™ Antibody Coupling Kit	Thermo Fisher Scientific	Cat#14311D
Goat serum	Sigma Aldrich	Cat#G9023
Griffonia (Bandeiraea) Simplicifolia Lectin I (GSL I, BSL I), Fluorescein	Vector Laboratories	Cat#FL-1101
M-MuLV Reverse Transcriptase	New England Biolabs Incorporation	Cat#M0253
QIAzol Lysis Reagent	Qiagen	Cat#79306
Random Primer Mix	New England Biolabs Incorporation	Cat#S1330S
RNase Inhibitor, Murine	New England Biolabs Incorporation	Cat#M0314S
Rodent Diet With 58 kcal% Fat and Sucrose	Research Diets	Cat#D12331
Streptavidin Particles Plus - DM	BD Biosciences	Cat#557812
SuperSignal™ West Pico PLUS Chemiluminescent Substrate	Thermo Fisher Scientific	Cat#34080
TaqMan™ Fast Advanced Master Mix	Thermo Fisher Scientific	Cat#4444963
VECTASHIELD Vibrance® Antifade Mounting Medium	Vector Laboratories	Cat#H-1700-10
phosphatase inhibitor PhosSTOP	Roche	#4906837001
cOmplete protease inhibitor	Roche	#11836153001

RESOURCE AVAILABILITY

Lead contact

Further information and requests for resources and reagents should be directed to and will be fulfilled by the lead contact, Tara L Haas (thaas@yorku.ca).

Materials availability

This study did not generate new unique reagents.

Data and code availability

- RNA sequencing data generated in this publication have been deposited in NCBI's Gene Expression Omnibus and are publicly available as of the date of publication. Accession numbers are listed in the key resources table.
- This paper does not report original code.
- Any additional information required to reanalyze the data reported in this paper is available from the lead contact upon request

EXPERIMENTAL MODEL AND SUBJECT DETAILS

Mice

Mouse protocols were approved by the York University Animal Care Committee and all experiments conformed to the standards of the Canadian Council on Animal Care. All mice were maintained in a 12:12 light:dark cycled, temperature-controlled environment with water and diet *ad libitum*. The first two cohorts of mice utilized genetically matched (FVB;B6) littermates that were bred in-house at York University and fed a high-fat diet (Surwit Diet, 58% kcal from fat, Research Diets) for a total of 7 weeks, starting at 7 weeks of

age. In the first cohort (n = 4 female and n = 4 male), subcutaneous and perigonadal white adipose tissues were harvested for whole tissue RNA analysis and EC isolation for RNA sequencing (RNA-Seq). In the second cohort, (n = 4 female, n = 3 male), mice were injected with EdU (*i.p.* 1.5 mg in 100 μL sterile PBS) on two sequential days prior to sacrifice and the perigonadal adipose tissue was used for whole-mount imaging analysis to detect proliferating cells. A third validation cohort of age-matched male and female C57Bl6/J mice (purchased from Jackson Laboratories) were fed a high fat diet for 7 weeks starting at 6 weeks of age (n = 6 males; 12 females). Perigonadal white adipose from this cohort of mice was used to isolate EC for qPCR validation of selected genes from the RNA-Seq dataset. C57Bl6/J mice were used to extend the validity of the RNAseq molecular signatures by testing in a difference mouse strain. To increase sample yield from the C57Bl6/J cohort, perigonadal adipose tissue from 2 females was pooled together for each EC isolation, yielding 6 independent RNA isolations for both females and males. Despite this strategy, the small amount of RNA yielded limited sample sizes for some gene expression analyses may show different sample sizes due to the small amount of starting material for RNA.

Primary murine endothelial cell cultures

EC were isolated from perigonadal white adipose tissue of male or female mice and purified with Streptavidin-magnetic beads coupled to biotinylated rat anti-mouse CD31 antibody.[9] Cells were used in experiments between passages 2 and 5.

METHOD DETAILS

Adipose EC isolation for RNA seq

Perigonadal and inguinal subcutaneous white adipose depots from each mouse were harvested, minced and digested with Type I collagenase (0.5% m/v) in DMEM for 30 min at 37°C (or until a single cell slurry was obtained). The resulting stromal vascular fraction was passed through a cell strainer (100 μm) and ECs were selected by incubation with Dynabeads conjugated to rat anti-mouse VE-cadherin antibody and Streptavidin-magnetic beads coupled to biotinylated rat anti-mouse CD31 antibody.[9]

Bulk RNA seq

RNA was extracted from freshly EC isolated from adipose tissues (pooled perigonadal and inguinal pads) using RNeasy Mini Kit and its quality was assessed using the RNA 6000 Nano chip on the 2100 Bioanalyzer automated electrophoresis system (Agilent Technologies Inc.). Samples with an RNA Integrity Number (RIN) > 6 (n = 4/group) were processed for RNA sequencing by The Centre for Applied Genomics, The Hospital of Sick Children, Toronto. PolyA-enriched cDNA-libraries were generated and sequenced using a Novaseq SP flowcell (paired end 2x50 bp), generating ~60 million reads per sample. After mapping reads to the mouse genome from Ensembl Mus_musculus.GRCm38.cdna.all.fa, expression levels were normalized as Transcripts Per Kilobase Per Million (TPKM) by dividing the read count of each transcript model with its length and scaling the total per sample to one million using Kalisto V0.4.4. Quality control of raw and mapped reads was done using FastQC version 0.11.8. Transcripts with <20 raw counts per library were deemed unexpressed and were discarded from analysis. Differential expression analysis was performed using the R package EdgeR version 3.34,[52] with the formula log2CPM = 0 + +Sex, correcting for common, trended and tagwise disparity. The analysis rendered two-base logarithmic fold change (log2FC) differences and false discovery rate (FDR) values, where FDR of <1% was considered significant.

Gene ontology and set enrichment analyses

Gene ontology analysis was performed using **D**atabase for **A**nnotation, **V**isualization and **I**ntegrated **D**iscovery (**DAVID**) v6.8[51,56] to identify enriched Biological Processes (BPs) within the genes significantly upregulated in male and female EC. Ontologies with a Benjamini p value < 0.05 were considered significant. Enrichplot (R)[53] was used to generate the dotplot based on the GO output. Gene set enrichment analysis (GSEA)[54] was used to test our RNA-Seq dataset for the enrichment of custom gene sets generated from literature. Customized gene sets included: endothelial tip cell markers[57,58]; proliferating EC markers[58–63]; oxidative phosphorylation[22]; inflammasome complex/NLRP3 inflammasome complex assembly (GO:0061702 and GO:0044546) and EC senescence associated secretory phenotype (SASP).[64–66] A .gmt file was created including all generated gene sets as mouse gene symbols, requiring no collapse or remapping in GSEA. The 14501 genes in our dataset were pre-ranked based on log fold change (positive values for genes upregulated in female, negative for those upregulated in males; zero cross at 7445). Gene sets with an FDR q-value<0.05 were considered significantly enriched.

Bioinformatic inference of transcriptional regulators

iRegulon,[48] accessed via Cytoscape,[50] was used to predict transcriptional regulators of the DEGs represented in the male-biased inflammatory ontologies (Immune System Process GO: 0002376; Positive Regulation of Phagocytosis GO: 0050766; Inflammatory Response GO: 0006954; Neutrophil Chemotaxis GO: 0030593; Antigen Processing and Presentation of Exogenous Peptide Antigen via MHC Class II GO: 0019886) and in the female-biased transcription and nucleosome assembly ontologies (Positive Regulation of Transcription GO:0045893; Nucleosome Assembly GO: 0006334). Transcription factor binding motifs were identified 10kB around the transcription start site.

Comparison with publicly available EC data

We also compared our RNA-Seq dataset with the sex-biased EC transcriptional profile of young and aged EC, compiled from multi-organ single cell sequencing analysis of 3- and 18-month-old mice from the Tabula Muris Senis dataset,[34] as compiled by Huang and colleagues.[33] To do this, we conducted GSEA of annotated Gene Ontology Biological Processes (GO BP) of each dataset, pre-ranking each dataset by log fold change. Gene sets were considered significantly enriched using FDR q values of <0.05, 0.1 and 0.15 for our dataset and the Huang datasets for young and aged-mice, respectively. The less stringent q value was utilized for the Huang dataset because this single cell sequencing dataset consisted of a much smaller number of genes (6,656 total) compared to our RNA-seq dataset (14,501 total). A clustering strategy was used to aid in describing similar ontologies comprised within each dataset. Biological networks were annotated using the "AutoAnnotate" function in Enrichment Map[67] (accessed via Cytoscape) and clustered according to the GLay clustering algorithm[68] based on ontology name. Only clusters containing five or more ontologies are reported. Lastly, we identified specific gene ontologies that were enriched in both datasets. The logFC and adjusted p values of selected genes comprising the leading edges of these shared gene sets were compared and displayed by chord plot.[49]

Whole-mount imaging of adipose tissue

Small pieces of formaldehyde-fixed perigonadal adipose tissue were stained to assess EC proliferation.[69] Proliferating endothelial cells (EdU+) were detected by pre-incubation in a solution containing 0.1 mM Azide-fluor 545; 0.1 M Tris, 1 mM $CuSO_4$, 0.1 M ascorbic acid prior to immunostaining. To visualize EC nuclei, samples were blocked and permeabilized with 0.1% Triton X-100, 5% goat serum in PBS followed by overnight incubation with rabbit anti-ERG (A7L1G) antibody (1:200), and 1 h incubation with Alexa Fluor647 goat anti-rabbit (1:200). Samples were counterstained with DAPI (1:1000) to detect all nuclei and *Griffonia simplicifolia* lectin I (GSL)-FITC (1:100) to detect capillaries. Single plane images were captured with a Zeiss LSM700 inverted confocal microscope equipped with a 40×/1.30 Oil EC PLAN-Neofluar objective (York University YSciCore). Microvascular content, EC nuclei and EdU positive nuclei were quantified from 4-5 fields of view per animal using ImageJ Analysis Software.

In vitro proliferation assays

Male and female adipose EC were plated in 96 well plates ($8x10^3$ cells per well). The following day, ECs were incubated for 4 h with 10 μM EdU (Click-iT EdU Imaging Kit) then fixed and Click reaction using Alexa Fluor488 Azide was performed according to the manufacturer's instructions. Cell nuclei were counterstained with DAPI (1:1000). Imaging and counting were performed using CellInsight CX7 High-Content Screening Platform (Thermo Fisher Scientific, USA) to quantify the number of EdU-positive and number of DAPI-positive cells, and the percentage of proliferating ECs was expressed as ($\#EdU^+$/ $\#DAPI^+$) x 100.

In vitro TNFα stimulation

Male and female adipose EC were plated at $4 x10^4$ cells per well in a 12-well plate. After 3 days, the media was replaced with 10% FBS high-glucose DMEM and then cells remained untreated, or stimulated with 5 ng/mL recombinant human TNFα, for 20 h before RNA extraction and analysis by qPCR.

RNA analysis by qPCR

RNA extracted from EC or whole adipose tissue was reverse transcribed using M-MLV reverse transcriptase and the cDNA was analyzed by real-time PCR on the Rotor-Gene Q platform (Qiagen Inc.) using Fast TaqMan Master Mix and TaqMan primers. Transcript levels of each target gene were calculated relative to an appropriate housekeeping gene (*Hprt1, Actb* or *Tbp)* and expressed as $2^{-\Delta Ct}$.

Western Blot analysis

Total protein extraction from cultured adipose EC was performed using lysis buffer containing 50 mM Tris (pH 8.0), 150 mM sodium chloride, 1% Nonidet P-40, 0.5% sodium deoxycholate, 0.1% sodium dodecyl sulfate with phosphatase inhibitor and protease inhibitor. Following protein separation through a polyacrylamide gel under reducing conditions, western blots were performed using the following primary antibodies: hexokinase 2 (HK2, 1:1,000), 6-phosphofructo-2-kinase/fructose-2,6-bisphosphatase 3 (PFKFB3, 1:1,000), and Glyceraldehyde-3-Phosphate Dehydrogenase (GAPDH, 1:1,000), Beta-actin (1:5,000) and alpha/beta Tubulin (1:1,000). Goat anti-rabbit or anti-mouse IgG-horseradish peroxidase secondary antibodies were utilized. Membranes were developed using enhanced chemiluminescence and densitometry analysis was performed with ImageJ Analysis Software (NIH).

QUANTIFICATION AND STATISTICAL ANALYSES

All data reported are from independent biological replicates with each mouse considered as one biological replicate. Averaged values were used when technical replicates (analysis of the same sample in duplicates) were performed. For *in vitro* assays, experiments were repeated at least six times with independent biological samples. No statistical methods were used to predetermine sample size, the experiments were not randomized and no outliers were excluded in our analyses. For 2-group comparisons, datasets with sample sizes greater than 6 were analyzed by unpaired Student's *t* test and those with samples sizes less than 6 were assessed using the nonparametric Mann-Whitney U test. Gene expression data from TNFα treatments of cultured cells were analyzed using 2-way repeated measures ANOVA (Sex x Treatment), followed by Sidak's multiple comparison post hoc tests when a significant main effect or interaction was identified. A p value of <0.05 was considered significant for all analyses, except for the DEG analysis for which a p value of <0.01 was the cut-off for significance. Statistical tests were performed using Prism ver. 5 or 7 (GraphPad Software Inc.). Data are shown as means $\pm$ standard errors of the mean (SEM) and p values are indicated in each Figure legend.